Applied Surface Science 269 (2013) 92–97

Contents lists available at SciVerse ScienceDirect

Applied Surface Science

journal homepage: www.elsevier.com/locate/apsusc

Characteristics of the electromagnetic interference shielding effectiveness of Al-doped ZnO thin films deposited by atomic layer deposition

Yong-June Choi[a], Su Cheol Gong[a], David C. Johnson[b], Stephen Golledge[b], Geun Young Yeom[c], Hyung-Ho Park[a,*]

[a] Department of Materials Science and Engineering, Yonsei University, Seoul 120-749, Republic of Korea
[b] CAMCOR, University of Oregon, Eugene, OR 97403-1241, USA
[c] Department of Advanced Materials Science and Engineering & SKKU Advanced Institute of Nanotechnology, Sungkyunkwan University, Suwon, Kyunggi-do 440-746, Republic of Korea

ARTICLE INFO

Article history:
Received 30 June 2012
Received in revised form
28 September 2012
Accepted 28 September 2012
Available online 5 October 2012

Keywords:
ZnO
Al-doped ZnO
Atomic layer deposition
Transparent conducting oxides
Electromagnetic shielding effectiveness

ABSTRACT

The structural, optical, and electrical properties of Al-doped ZnO (ZnO:Al) thin films deposited by atomic layer deposition (ALD) with a modified precursor pulse sequence were investigated to evaluate the electromagnetic interference shielding effectiveness (EMI-SE). A Zn–Al–O precursor exposure sequence was used in a modified ALD procedure to result in better distribution of Al^{3+} ions in the ZnO matrix with the aim of reducing the formation of complete nano-laminated structures that may form in the typical alternating ZnO and Al_2O_3 deposition procedure. The ALD dopant concentration of the ZnO:Al films was varied by adjusting the dopant deposition intervals of the ZnO:Zn—Al—O precursor pulse cycle ratios among 24:1, 19:1, 14:1, and 9:1. The lowest obtained resistivity and average transmittance in the visible region (380-780 nm) were $5.876 \times 10^{-4}\ \Omega$ cm (carrier concentration of 6.02×10^{20} cm^{-3} and Hall mobility of 17.65 cm^2/V s) and 85.93% in the 131 nm thick ZnO:Al(19:1) film, respectively. The average value of the EMI-SE in the range of 30 MHz to 1.5 GHz increased from 1.1 dB for the 121 nm thick undoped ZnO film to 6.5 dB for the 131 nm thick ZnO:Al(19:1) film.

1. Introduction

Zinc oxide (ZnO) has been actively explored as a promising alternative material to indium tin oxide (ITO), which has drawbacks such as the exhaustion of natural indium sources and its toxicity. ZnO, which is an n-type, wide band gap transparent oxide semiconductor (3.27 eV at room temperature) possessing a high exciton binding energy of 60 meV [1], has recently attracted attention for applications involving transparent electrodes in solar cells and transparent thin film transistors because it is non-toxic, inexpensive, highly abundant, and stable in hydrogen plasma, compared to ITO [2]. However, due to the low conductivity of ZnO compared to ITO, doping with trivalent metal cations (Group III elements; B, Al, and Ga) has been investigated while focusing on regulating the doping levels [3]. Because group III elements generally have same valencies but smaller ionic sizes than the host Zn^{2+} cation, it is theoretically explained that extrinsic dopants substitute into host Zn sites and provide an extra electron. Among cation-doped ZnO films, Al-doped ZnO (ZnO:Al) has been intensively investigated in recent years. Agura et al. reported the lowest resistivity of $8.5 \times 10^{-5}\ \Omega$ cm with extremely high carrier concentration of 1.5×10^{21} cm^{-3} for ZnO:Al films deposited by pulsed laser deposition (PLD) [4]. Moreover, many research groups reported the electrical properties of ZnO:Al films in order to apply to electronic devices due to high carrier concentration of ZnO:Al films [5–8].

Several techniques are used for the fabrication of ZnO thin films including sol–gel, spray pyrolysis, sputtering, e-beam evaporation, chemical vapor deposition, and atomic layer deposition (ALD) methods [9]. In particular, ALD technique is a thin film growth method by a self-limiting surface chemistry composed with repeating process of pulse and purge with precursors, and also keeping the source materials separately during whole depositing process. Therefore, ALD can allow low temperature growth, better step coverage (high-aspect-ratio), good uniformity, and controllability of the film thickness by controlling the number of ALD cycles. Moreover, separate dosing of the precursors prevents gas phase reactions, which allows the use of highly reactive precursors and provides sufficient time for each reaction step to reach completion. These excellent properties allow the deposition of electronic devices with a complex 3D structure and processing at relatively low temperatures, facilitating the use of flexible substrates [10].

The introduction of an optimum amount of Al to the ZnO matrix results in a marked increase of the electrical conductivity while the optical properties remain excellent with a slight increase of

* Corresponding author. Tel.: +8 2 2123 2853; fax: +82 2 312 5375.
E-mail address: hhpark@yonsei.ac.kr (H.-H. Park).

0169-4332/$ – see front matter © 2012 Elsevier B.V. All rights reserved.
http://dx.doi.org/10.1016/j.apsusc.2012.09.159

Table 1
Sample identification (I.D.), DEZ/H2O (DH):DEZ/TMA/H2O (DTH) cycle ratio, number of ZnO monolayers (*N*) during one super cycle, film thicknesses measured by SEM, and Al atomic contents of the ZnO:Al films obtained by EDS.

I.D.	DH:DTH cycle ratio	*N*	Total number of super cycles	Thickness (nm) (via SEM)	at.% Al (via EDS)
ZnO	–	667	–	121	0
R_{24}	DH 24:DTH 1	24	32	132	1.7
R_{19}	DH 19:DTH 1	19	40	131	2.1
R_{14}	DH 14:DTH 1	14	53	126	2.9
R_9	DH 9:DTH 1	9	80	130	4.7

transmittance due to the band gap widening effect [11]. In ZnO:Al films formed using ALD, most researchers typically use ZnO/Al_2O_3 nano-laminated structures for doping Al^{3+} ions into the ZnO matrix [12]. In ZnO:Al films deposited by this conventional process, however, it is very difficult to uniformly distribute the Al dopant into the ZnO matrix by ALD due to the huge gap between the numbers of ZnO and Al_2O_3 cycles. To address this problem, we demonstrated an effective ALD procedure for uniform dopant distribution in our previous work [13]. Therein, a uniform dopant distribution was confirmed by secondary ion mass spectrometry using an O^{2-} ion source, while the chemical bonding state of Al dopant in ZnO matrix was analyzed by photoemission spectroscopy.

With an increase in the use of mobile electronic devices, the level of interest in electromagnetic interference (EMI) shielding has grown in recent years. EMI shielding materials are commonly used with metals, metal powder, metal-fiber filled plastics, and metal-reinforced polymers [14–16]. In the case of metals, however, there are some limitations such as corrosion susceptibility, long processing time, high cost of equipment for production, and also the difficulty of deposition on transparent electronic devices. In the case of polymer composite materials, they are weakly resistant to moisture and have mechanical strength issues although many limitations of metal-related materials can be overcome. However, due to the lack of EMI shielding applications of transparent conducting oxides (TCOs), less attention has so far been paid to EMI shielding properties of TCO films even though they have many merits compared with metals and polymer materials. Therefore, in this study, undoped ZnO and ZnO:Al films were investigated to apply in transparent EMI shielding materials as an alternative to metal and polymer composites because it has adequate transparency and conducting properties for reflection and absorption of EMI radiation. Furthermore, a modified precursor pulse sequence was adopted and the properties of ZnO:Al thin films with varying compositions deposited using this sequence were determined for applications in transparent EMI shielding materials used in mobile electric devices.

2. Experimental details

Undoped ZnO and ZnO:Al thin films were deposited on Si(1 0 0) wafers and glass (Fusion 1737) substrates via ALD using a traveling wave type Lucida D100 system (NCD Technology, Inc., Korea) at a deposition temperature of 250 °C and a working pressure of 3–3.3 Torr. Diethylzinc (DEZ, Hansol Chemical Co., Ltd., Korea) and trimethylaluminum (TMA, Hansol Chemical Co., Ltd., Korea) were used as the precursors for Zn and Al, respectively, and deionized water (H_2O) was used as a reactant. DEZ and TMA were delivered into the chamber with a high purity N_2 (99.999%) carrier gas flow of 20 sccm (standard cubic centimeters per minute). The ZnO films were typically deposited by DEZ-H_2O cycles with following sequence: DEZ pulse 0.1 s → N_2 purge 10 s → H_2O pulse 0.1 s → N_2 purge 10 s. For Al-doping into the ZnO matrix, most of the deposition is ordinarily composed with the combination of the DEZ-H_2O cycles of ZnO and TMA-H_2O cycles of Al_2O_3 with following conventional sequence: TMA pulse 0.1 s → N_2 purge 10 s → H_2O pulse 0.1 s → N_2 purge 10 s. To avoid the formation of ZnO:Al films by a ZnO/Al_2O_3 nanolaminate structure and improve uniform dopant contribution, we conducted modified sequence for fabrication of ZnO:Al films in this work: DEZ pulse 0.1 s → N_2 purge 10 s → TMA pulse 0.1 s → N_2 purge 10 s → H_2O pulse 0.1 s → N_2 purge 10 s. The details of the fabrication method and operating conditions of the conventional and modified ZnO:Al thin films are provided in our previous publication [13]. For the deposition of ZnO:Al films, various numbers of ZnO ALD cycles (*N*) and one modified Zn—Al—O ALD cycle were repeatedly carried out for a total of 800 ALD cycles (except for the R_{14} samples, which had 795 ALD cycles). This allowed us to manipulate the doping concentration (Table 1).

The phase and crystallinity of the films were monitored by X-ray diffraction (XRD; Rigaku Ultima IV) with Cu Kα radiation (λ = 1.5418 Å). The electrical properties of the films were measured using the van der Pauw method at room temperature using a Hall effect measurement system (Ecopia HMS3000). The electrical parameters were measured by the direct current (I_{DC} = 10–1 mA) four probe method in a magnetic field strength of up to 0.57 T. Scanning electron microscopy (SEM; JEOL, JSM 7001F) was used to observe the morphologies of the ALD-grown thin films and to measure the final thicknesses of the films via cross-sectional images. Energy dispersive spectroscopy (EDS) was used to quantify the Al content in the ZnO:Al thin films. Optical transmittance measurements were conducted using an ultraviolet-visible-near infrared (UV-vis-NIR) spectrophotometer (V-570, JASCO). The EMI shielding effectiveness (SE) was tested by the ASTM (American Society for Testing and Materials) D4953-99 method, which is commonly used for the measurement of the EMI-SE as a global standard. By using ASTM D4953-99, the EMI-SE of the films was measured using a Network Analyzer 4396B (Agilent Technologies) with a flanged circular coaxial transmission line holder. The measured frequencies ranged from 30 MHz to 1.5 GHz. Fig. 1 shows the dimensions of the specimens and ALD-deposited samples used in measuring the EMI-SE of the films where Fig. 1(a) and (b) show a reference sample and load sample, respectively. The EMI-SE values in terms of decibels (dB) were calculated using the following equation,

$$\text{EMI-SE (dB)} = 10 \log \left(\frac{P_{out}}{P_{in}} \right) \quad (1)$$

where dB is the unit of the power ratio, typically used to specify shielding effectiveness, P_{out} is the output power (Watts), and P_{in} is the input power (Watts) [17].

3. Results and discussion

To confirm the deposition rates of the ALD-ZnO:Al thin films, the film growth behaviors of individual ZnO and Al_2O_3 films were investigated. The thicknesses of the undoped ZnO and ZnO:Al films are given in Table 1 which remained relatively constant as a function of the number of ALD cycles in the range of 121–132 nm, indicating the self-limiting conditions for ALD growth. The film growth rates of the Al_2O_3, ZnO, and ZnO:Al(R_{19}) films were 1.2 Å/cycle, 1.8 Å/cycle, and 1.6 Å/cycle, respectively. These growth rates of the ALD-grown materials are in the range of other results,

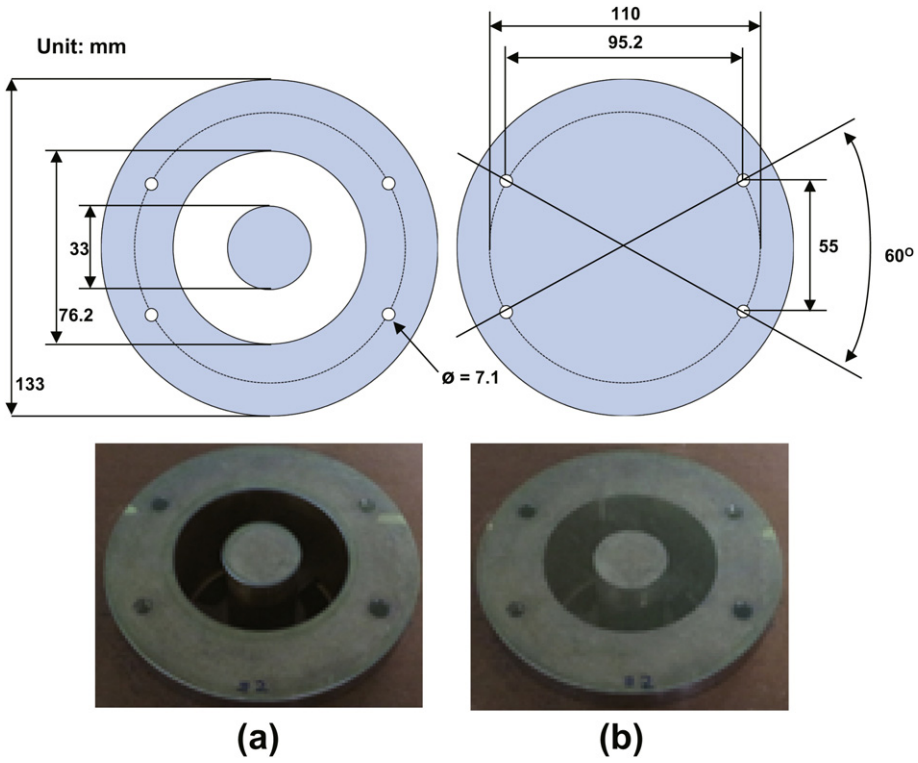

Fig. 1. Dimensions and pictures of (a) reference and (b) load specimens for the ASTM D4935-99 EMI-SE test.

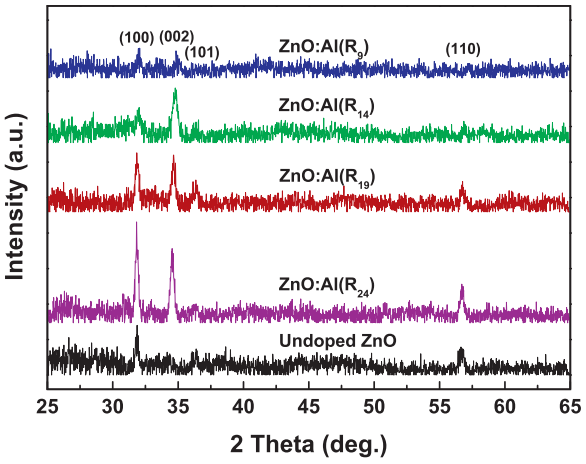

Fig. 2. XRD patterns of undoped ZnO and various ALD cycle ratio Al-doped ZnO films deposited by ALD.

which ranged from 1.3 Å/cycle to 2.0 Å/cycle for ZnO and from 0.8 Å/cycle to 1.3 Å/cycle for Al_2O_3 [12,18,19].

The XRD patterns of undoped ZnO and ZnO:Al films on glass substrates with various cycle ratios are shown in Fig. 2. All films exhibited a hexagonal wurtzite structure with visible (1 0 0), (0 0 2), (1 0 1), and (1 1 0) peaks. Crystalline Al_2O_3 or $ZnAl_2O_4$ peaks were not visible, indicating that phase segregation of the films with doping of Al into the ZnO matrix did not occur under our experimental conditions. The peak positions of all films, however, changed slightly to higher angles with increasing Al content. This phenomenon is generally known as lattice distortion, as the introduction of Al^{3+} ions substitutes for Zn^{2+} ions. Further, with increasing Al concentration, a predominant peak change from (1 0 0) to (0 0 2) was observed and the crystallinity of the films was noticeably degraded [20]. In the equilibrium state, if there is no influence of epitaxy, the film grows in the plane of the lowest surface free energy parallel to the surface below the roughening temperature [21]. However, with increasing Al content, the lowest free energy plane changed to the (0 0 2) plane under our experimental conditions due to lattice distortion of the ZnO matrix with the substitutional Al^{3+} ions (0.54 Å), which have a smaller ionic radius than Zn^{2+} ions (0.74 Å) [22]. With increasing Al content, SEM images were obtained to observe the surface morphologies and thickness of the films, as shown in Fig. 3. The grain boundaries of oxide semiconductor ZnO films act as trap-sites due to negatively charged O species, forming a potential barrier. Therefore, the negatively charged O species form depletion regions near the grain boundaries and result in decreases of the carrier concentration and Hall mobility of the films. Based on this aspect, the surface morphologies of the ZnO:Al(R_{24}), ZnO:Al(R_{19}), and ZnO:Al(R_{14}) films were investigated and they were found to have larger grain sizes than the ZnO and ZnO:Al(R_9) films, which was also indicated by the XRD patterns of the films.

Fig. 4(a) shows the optical transmittance of the undoped ZnO and various ZnO:Al films. The average transmittance values in the visible region (from 380 to 780 nm) of the undoped ZnO, ZnO:Al(R_{24}), ZnO:Al(R_{19}), ZnO:Al(R_{14}), and ZnO:Al(R_9) films were 82.92%, 85.25%, 85.93%, 86.23%, and 86.40%, respectively. Similar to other reported results [23], the optical transmittance of the ZnO:Al films was slightly enhanced with increasing Al content in the range from 380 to 480 nm. This result could be explained by more facile electron transition for absorbing photon energy in the short wavelength region with increasing Al metal cation concentration in the ZnO matrix [24]. This high transmittance value is suitable for transparent EMI shielding materials because the average transmittance values were always greater than 85% [25].

The absorption coefficient was calculated using Lambert's formula,

$$\alpha = \frac{1}{t[\ln(1/T_r)]} \quad (2)$$

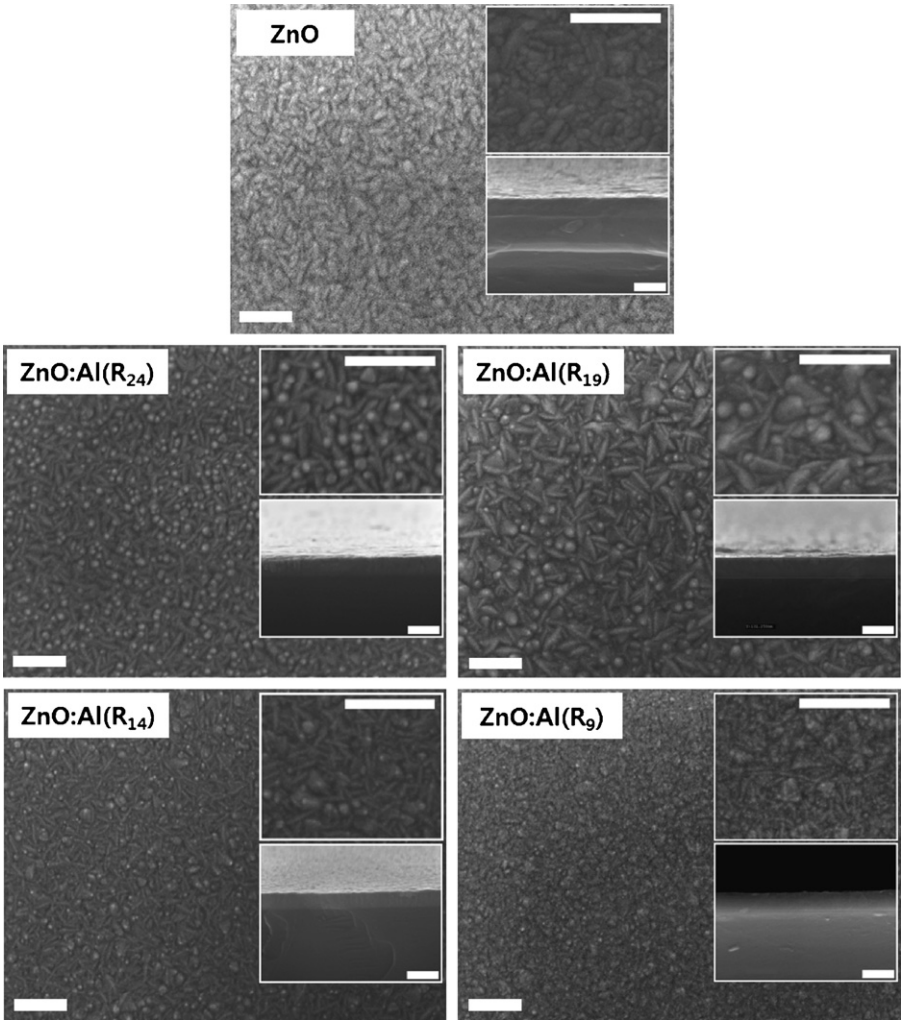

Fig. 3. Surface morphologies of undoped ZnO and various ALD cycle ratio Al-doped ZnO films deposited by ALD. Upper and below insets are indicated enlarged and cross-sectional images, respectively (all the scale bars are represented by 200 nm).

where T_r and t are the transmittance and film thickness, respectively [26]. The direct band gaps of the films were estimated from the $(\alpha h\nu)^2$ vs. $h\nu$ (Tauc relation) plot by extrapolating a fit of the linear region to $\alpha = 0$, as shown in Fig. 4(b). The estimated optical band gap values increased with increasing Al content and the values of the undoped ZnO, ZnO:Al(R_{24}), ZnO:Al(R_{19}), ZnO:Al(R_{14}), and ZnO:Al(R_9) films were 3.27 eV, 3.39 eV, 3.48 eV, 3.57 eV, and 3.69 eV, respectively. Further, the shift in the absorption edge increased with increasing Al content. The band gap of the ZnO film, 3.27 eV, agrees well with the ideal band gap of pure ZnO [1] and the increase in the band gap with increasing Al content is normally due to the Burstein–Moss effect [27,28]. ZnO films are naturally n-type oxide semiconductors due to natural electron donors generated by O vacancies and Zn interstitials. The addition of donor Al^{3+} cations raises the Fermi level of the ZnO:Al films into the conduction band, causing the films to completely degenerate. Therefore, the absorption edge moves to higher energies than the actual band gap of pure ZnO. The carrier concentration, Hall mobility, and resistivity values of the undoped ZnO, ZnO:Al(R_{24}), ZnO:Al(R_{19}), ZnO:Al(R_{14}), and ZnO:Al(R_9) films are shown in Fig. 5(a) and (b). The lowest and highest resistivity values were $5.876 \times 10^{-4}\ \Omega$ cm for ZnO:Al(R_{19}) and $2.310 \times 10^{-3}\ \Omega$ cm for undoped ZnO, respectively. As Al is incorporated into the ZnO matrix, the Hall mobility decreased from 29.19 cm^2/V s to 6.24 cm^2/V s and the carrier concentration increased from $9.3 \times 10^{19}\ cm^{-3}$ to $6.8 \times 10^{20}\ cm^{-3}$. Many other reports regarding ZnO:Al films reported similar tendencies or a decrease of resistivity with the introduction of Al up to a certain concentration before increasing thereafter [29]. The optimum Al concentration was 2.1 at.%, ZnO:Al(R_{19}), which was deposited using a number of super cycles consistent with a DEZ/H_2O:DEZ/TMA/H_2O cycle ratio of 19:1, as mentioned in the experimental section. This optimum concentration was within the range of previously reported values. In particular, Elam et al. reported almost the same tendency in which the lowest resistivity was obtained from a 19:1 ZnO:Al film obtained using a conventional deposition process [12].

Fig. 6 shows the EMI-SE test results of the bare glass, undoped ZnO, and ZnO:Al(R_{19}) films. In order to evaluate the influence of the glass substrate, the EMI-SE test was performed for the bare glass substrate. As expected, the EMI-SE value of the glass substrate was 0 dB and therefore, the influence of the substrate could be ignored in our experiments. The EMI-SE value for the 121 nm thick undoped ZnO film and the 131 nm thick ZnO:Al(R_{19}) film were 1.1 dB and 6.5 dB, respectively, in the measured frequency range (30 MHz to 1.5 GHz). The EMI-SE value of the ZnO:Al(R_{19}) film was dramatically higher by a factor of 6 compared to the undoped ZnO film. This fact can be explained by typical mechanism of EMI shielding. The primary mechanism of EMI shielding is reflection of radiation through the mobile charge carrier (electrons and/or holes) in the films and a second mechanism is the absorption by electric and/or magnetic dipole of shielding materials [30]. In our case, reflection

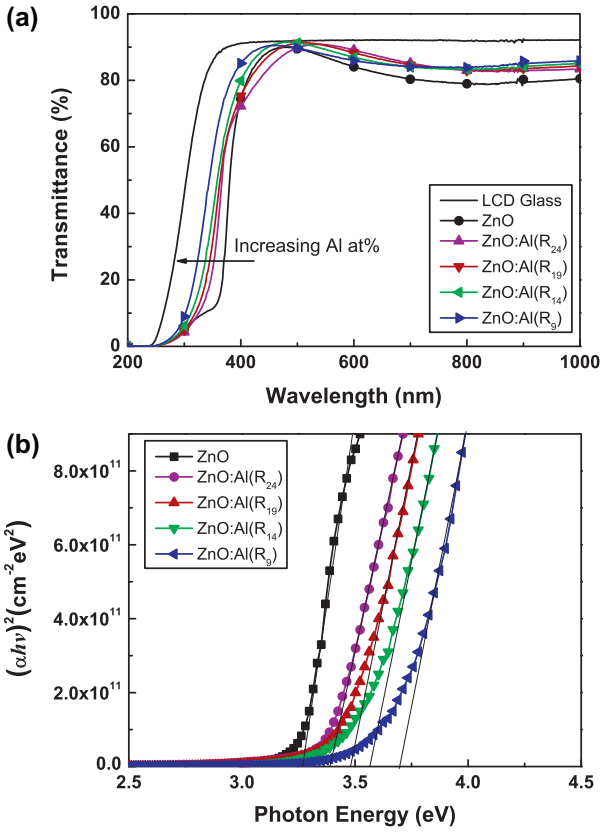

Fig. 4. (a) Transmission spectra and (b) evaluated optical band gap of undoped ZnO and various ALD cycle ratio Al-doped ZnO films deposited by ALD.

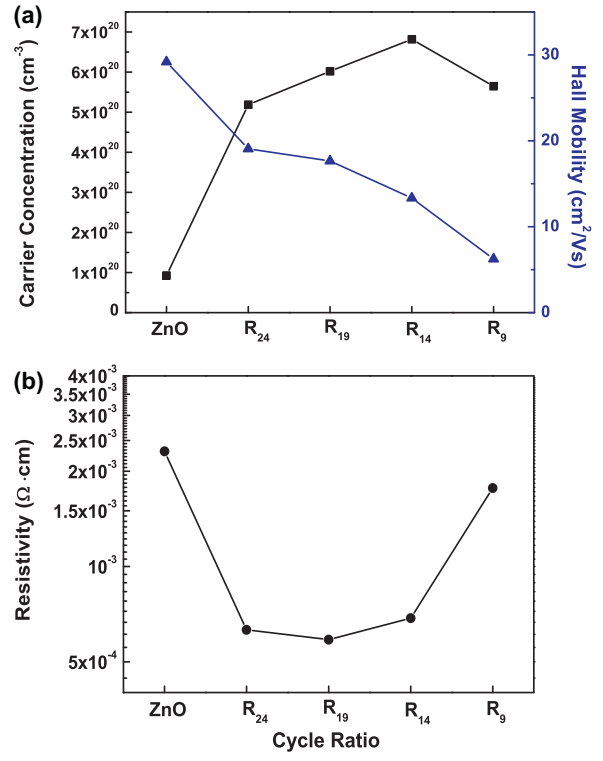

Fig. 5. (a) Carrier concentration (■), Hall mobility (▲), and (b) resistivity (●) of undoped ZnO and various ALD cycle ratio Al-doped ZnO films as a function of the ALD cycle ratio.

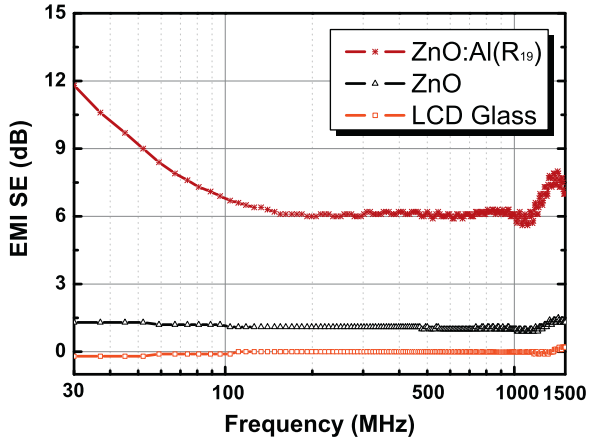

Fig. 6. EMI-SE values of bare glass, undoped ZnO, and ZnO:Al(R19) films as a function of the frequency in the range of 30 MHz to 1.5 GHz (Table 1). Sample identification (I.D.), DEZ/H_2O (DH):DEZ/TMA/H_2O (DTH) cycle ratio, number of ZnO monolayers (*N*) during one super cycle, film thicknesses measured by SEM, and Al atomic contents of the ZnO:Al films obtained by EDS.

is a dominant factor for the increase of the EMI-SE because ZnO has a relatively low dielectric constant for absorption of radiation. This can be confirmed by comparing the measured EMI-SE with the calculated value considering the relative amount of carriers. When considering the thickness (8% thicker for the ZnO:Al(R_{19}) film) and carrier concentration (731% richer for the ZnO:Al(R_{19}) film) of the undoped ZnO and ZnO:Al(R_{19}) films, a 6.77 times larger EMI-SE could be expected for the ZnO:Al(R_{19}) film compared to the undoped ZnO film, which is comparable to the measured result which was 6 times larger. From the above results, reflection is a dominant factor for the EMI shielding effect of ZnO films and application to transparent EMI shielding materials may be expected through proper control of the ZnO:Al film thickness.

4. Conclusions

We studied the structural, optical, and electrical properties of ZnO:Al thin films with thicknesses ranging from 121 to 132 nm for applications as transparent EMI shielding materials. The XRD results showed that the increasing Al concentration resulted in a predominant peak change from (1 0 0) to (0 0 2). The average optical transmittance was greater than 85% in the visible range with an absorption edge shift due to the Burstein–Moss shift. The lowest resistivity was 5.876×10^{-4} Ω cm with an Al content of 2.1 at.% in the 132 nm thick ZnO:Al(R_{19}) thin film and the corresponding EMI-SE value was 6.5 dB in the measured frequency range (30 MHz to 1.5 GHz). The reflection was found to be a dominant factor for the EMI shielding effect of the ZnO films. Based on the results of this study, we suggest that the optical and electrical properties of ZnO:Al films can be optimized by controlling the modified cycle ratio. Also, transparent conducting oxide thin films can be applied to EMI shielding materials. Therefore, these films have potential for use in transparent EMI shielding windows of optoelectronic devices such as mobile phones.

Acknowledgement

This work was supported by the Industrial Strategic Technology Development Program (10041926, development of high density plasma technologies for thin film deposition of nanoscale semiconductor and flexible display processing) funded by the Ministry of Knowledge Economy (MKE, Korea).

References

[1] D.S. Ginley, C. Bright, Transparent conducting oxides, MRS Bull. 25 (2000) 15–18.
[2] H. Fan, S.A. Reid, Phase transformations in pulsed laser deposited nanocrystalline tin oxide thin films, Chem. Mater. 15 (2003) 564–567.
[3] D.-J. Lee, H.-M. Kim, J.-Y. Kwon, H. Choi, S.-H. Kim, K.-B. Kim, Structural and electrical properties of atomic layer deposited Al-doped ZnO films, Adv. Funct. Mater. 21 (2011) 448–455.
[4] H. Agura, A. Suzuki, T. Matsushita, T. Aoki, M. Okuda, Low resistivity transparent conducting Al-doped ZnO films prepared by pulsed laser deposition, Thin Solid Films 445 (2003) 263–267.
[5] C. Hao, B. Xie, M. Li, H. Wang, Y. Jiang, Y. Song, The influence of high energetic oxygen negative ions and active oxygen on the microstructure and electrical properties of ZnO:Al films by MF magnetron sputtering, Appl. Surf. Sci. 258 (2012) 8234.
[6] T.L. Chen, D.S. Ghosh, D. Krautz, S. Cheylan, V. Pruneri, Highly stable Al-doped ZnO transparent conductors using an oxidized ultrathin metal capping layer at its percolation thickness, Appl. Phys. Lett. 99 (2011) 093302.
[7] G.B. Murdoch, S. Hinds, E.H. Sargent, S.W. Tsang, L. Mordoukhovski, Z.H. Lu, Aluminum doped zinc oxide for organic photovoltaics, Appl. Phys. Lett. 94 (2009) 213301.
[8] F. Ruske, M. Roczen, K. Lee, M. Wimmer, S. Gall, J. Hüpkes, D. Hrunski, B. Rech, Improved electrical transport in Al-doped zinc oxide by thermal treatment, J. Appl. Phys. 107 (2010) 013708.
[9] T. Minami, Transparent conducting oxide semiconductors for transparent electrodes, Semicond. Sci. Technol. 20 (2005) S35–S44.
[10] M. Leskelä, M. Ritala, Atomic layer deposition chemistry: recent developments and future challenges, Angew. Chem. Int. Ed. 42 (2003) 5548–5554.
[11] T. Minami, S. Suzuki, T. Miyata, Transparent conducting impurity-co-doped ZnO:Al thin films prepared by magnetron sputtering, Thin Solid Films 398–399 (2001) 53–58.
[12] J.W. Elam, S.M. George, Growth of ZnO/Al_2O_3 alloy films using atomic layer deposition techniques, Chem. Mater. 15 (2003) 1020–1028.
[13] J.Y. Kim, Y.-J. Choi, H.-H. Park, S. Golledge, D.C. Johnson, Effective atomic layer deposition procedure for Al-dopant distribution in ZnO thin films, J. Vac. Sci. Technol. A 28 (2010) 1111–1114.
[14] A. Kaynak, Electromagnetic shielding effectiveness of galvanostatically synthesized conducting polypyrrole films in the 300–2000 MHz frequency range, Mater. Res. Bull. 31 (1996) 845–860.
[15] K.B. Cheng, M.L. Lee, S. Ramakrishna, T.H. Ueng, Electromagnetic shielding effectiveness of stainless steel/polyester woven fabrics, Text. Res. J. 71 (2001) 42–49.
[16] S.K. Dhawan, N. Singh, D. Rodrigues, Electromagnetic shielding behavior of conducting polyaniline composites, Sci. Technol. Adv. Mater. 4 (2003) 105–113.
[17] N.C. Das, D. Khastgir, T.K. Chaki, A. Chakraborty, Electromagnetic interference shielding effectiveness of carbon black and carbon fibre filled EVA and NR based composites, Compos. A: Appl. Sci. Manuf. 31 (2000) 1069–1081.
[18] M.D. Groner, F.H. Fabreguette, J.W. Elam, S.M. George, Low-temperature Al_2O_3 atomic layer deposition, Chem. Mater. 16 (2004) 639–645.
[19] E. Guziewicz, I.A. Kowalik, M. Godlewski, K. Kopalko, V. Osinniy, A. Wójcik, S. Yatsunenko, E. Łusakowska, W. Paszkowicz, M. Guziewicz, Extremely low temperature growth of ZnO by atomic layer deposition, J. Appl. Phys. 103 (2008) 033515.
[20] S. Yoshioka, F. Oba, R. Huang, I. Tanaka, T. Mizoguchi, T. Yamamoto, Atomic structures of supersaturated $ZnO–Al_2O_3$ solid solutions, J. Appl. Phys. 103 (2008) 014309.
[21] W.K. Burton, N. Cabrera, F.C. Frank, The growth of crystals and the equilibrium structure of their surfaces, Philos. Trans. R. Soc. A: Math. Phys. Eng. Sci. 243 (1951) 299–358.
[22] S.-Y. Pung, K.-L. Choy, X. Hou, C. Shan, Preferential growth of ZnO thin films by the atomic layer deposition technique, Nanotechnology 19 (2008) 435609.
[23] P. Banerjee, W.-J. Lee, K.-R. Bae, S.B. Lee, G.W. Rubloff, Structural, electrical, and optical properties of atomic layer deposition Al-doped ZnO films, J. Appl. Phys. 108 (2010) 043504.
[24] S. Qu, Y. Song, H. Liu, Y. Wang, Y. Gao, S. Liu, X. Zhang, Y. Li, D. Zhu, A theoretical and experimental study on optical limiting in platinum nanoparticles, Opt. Commun. 203 (2002) 283–288.
[25] T.G. Kryshtab, J. Palacios Gómez, M.O. Mazin, Phenomenon of primary and secondary extinction in textured materials, Rev. Mex. Fis. 48 (2002) 100–106.
[26] S.T. Tan, B.J. Chen, X.W. Sun, W.J. Fan, H.S. Kwok, X.H. Zhang, S.J. Chua, Blueshift of optical band gap in ZnO thin films grown by metal-organic chemical-vapor deposition, J. Appl. Phys. 98 (2005) 013505.
[27] E. Burstein, Anomalous optical absorption limit in InSb, Phys. Rev. 93 (1954) 632–633.
[28] T.S. Moss, The interpretation of the properties of indium antimonide, Proc. Phys. Soc. B 67 (1954) 775–782.
[29] J.-S. Na, G. Scarel, G.N. Parsons, In situ analysis of dopant incorporation, activation, and film growth during thin film ZnO and ZnO:Al atomic layer deposition, J. Phys. Chem. C 114 (2010) 383–388.
[30] D.D.L. Chung, Electromagnetic interference shielding effectiveness of carbon materials, Carbon 39 (2001) 279–285.